Resolving discrepancies between LEED and STM through *ab initio* calculations: Surface and bonding of sulfur on Mo(110)

M. Chen, P. G. Clark, Jr., T. Mueller, and C. M. Friend*
Department of Chemistry, Harvard University, Cambridge, Massachusetts 02138

Efthimios Kaxiras
Department of Physics and Division of Engineering and Applied Sciences, Harvard University, Cambridge, Massachusetts 02138
(Received 18 March 1999; revised manuscript received 28 May 1999)

The adsorption of sulfur at 0.5 ML in both $c(2\times2)$ and $\left[\begin{smallmatrix}2 & \bar{2}\\ 1 & 1\end{smallmatrix}\right]$ configurations on the Mo(110) surface is studied using the density-functional, pseudopotential method with a plane-wave basis and a seven-layer slab geometry in conjunction with scanning tunneling microscopy (STM) and low-energy electron diffraction (LEED) experiments. The sulfur adatoms are placed in different possible binding sites in order to determine the most favorable adsorption site. The $\left[\begin{smallmatrix}2 & \bar{2}\\ 1 & 1\end{smallmatrix}\right]$ overlayer is more stable than the $c(2\times2)$ by 0.31 eV, in agreement with experiment. The greater stability of the $\left[\begin{smallmatrix}2 & \bar{2}\\ 1 & 1\end{smallmatrix}\right]$ structure is attributed to differences in metal-metal bonding. Sulfur is predicted to adsorb at a low-symmetry position near the long-bridge site; the long-bridge site is slightly less favorable in energy. Simulated STM images of the sulfur-covered surface are constructed, and found to model well the experimental images. We find that the bright areas in the calculated STM images do not necessarily correspond to the position of the sulfur atoms, which explains the difference between the LEED pattern and the experimentally observed STM images. [S0163-1829(99)02340-1]

INTRODUCTION

The adsorption of sulfur on Mo(110) is of interest in several areas of surface science. This system has been used as a model for studying MoS_2-based hydrodesulfurization catalysts; moreover, the variety of surface structures of sulfur on Mo(110) has been studied in the context of two-dimensional structural phase transitions.[1,2] This system has been studied extensively with traditional surface-science techniques, including low-energy electron diffraction (LEED), Auger electron spectroscopy, and scanning tunneling microscopy (STM). A number of different ordered surface structures of sulfur on Mo(110) have been observed by LEED: $p(2\times2)$, (7×1), (4×1), (1×5), (1×3), and (1×10), corresponding to coverages of 0.25, 0.43, 0.5, 0.6, 0.66, and 0.7 ML, respectively.[1–4]

A tensor LEED analysis of the $p(2\times2)$ phase indicated that the most favorable binding site for the sulfur was displaced 0.03 Å away from the long bridge towards the quasithreefold site.[4] Furthermore, the sulfur induced buckling of some surface Mo atoms, by as much as 0.2 Å, based on the LEED analysis.

Although the structures of other phases are not known in detail, the local binding of sulfur is expected to be qualitatively similar to the $p(2\times2)$ phase. Variations in the exact bond distances and the degree of buckling are expected. In order to obtain insight into both the bonding and structure of sulfur on Mo(110), we have combined first-principles electronic-structure calculations with scanning tunneling microscopy. By simulating STM images using the electronic-structure calculations, we are also able to resolve an apparent discrepancy between the $\left[\begin{smallmatrix}2 & \bar{2}\\ 1 & 1\end{smallmatrix}\right]$ LEED pattern and the experimental STM images which have $c(2\times2)$ symmetry. Our results demonstrate that bright spots in the STM do not necessarily correspond to atomic positions of the adsorbate atoms. This is discussed in light of related results for sulfur on other surfaces. Finally, we perform calculations for and discuss the properties of the related $c(2\times2)$ phase, which is not observed experimentally, in order to elucidate the origin of the $\left[\begin{smallmatrix}2 & \bar{2}\\ 1 & 1\end{smallmatrix}\right]$ structure.

CALCULATION DETAILS

All calculations were performed using a commercially available plane-wave, density-functional code, CASTEP, in which the Kohn-Sham equations are solved self-consistently.[5,6] The core electrons of Mo and S were represented by ultrasoft pseudopotentials,[7,8] which allow a cutoff of 290 eV to be used for the plane-wave basis set. The exchange-correlation energy is calculated in the local-density approximation, using the parametrization of Perdew and Zunger.[9] The electronic density was relaxed to the ground state using Pulay mixing,[10,11] and the Hamiltonian was iteratively diagonalized with a conjugate gradient scheme.

The Mo(110) surface was represented by a symmetric seven-layer slab; in all calculations the middle three layers were fixed to the bulk positions. Using this model, a calculation of the clean seven-layer slab produced a top-layer contraction of 7% and a second-layer contraction of 1%, which compares well with other calculations of the Mo(110) surface.[12,13] Sulfur was adsorbed on both sides of the Mo slab in a $c(2\times2)$ or a $\left[\begin{smallmatrix}2 & \bar{2}\\ 1 & 1\end{smallmatrix}\right]$ configuration, which corresponds to a 0.5-ML coverage, resulting in two Mo atoms and one S atom per surface unit cell for the $c(2\times2)$ case, and four Mo atoms and two S atoms per surface unit cell for the $\left[\begin{smallmatrix}2 & \bar{2}\\ 1 & 1\end{smallmatrix}\right]$

configuration. The slabs were separated by 13 Å of vacuum. In the directions parallel to the surface, the experimental lattice constants were used. The free atoms in the slab were relaxed until the average force on each atom was less than 0.05 eV/Å. The Brillioun zone was sampled at 15 special **k** points generated according to the scheme of Monkhorst and Pack, corresponding to 9 special **k** points in the irreducible Brillioun zone for the $c(2\times2)$ unit cell and 4 special **k** points in the irreducible Brillioun zone for the $\begin{bmatrix} 2 & \bar{2} \\ 1 & 1 \end{bmatrix}$ unit cell. In order to find the most favorable binding site for sulfur on Mo(110), the $c(2\times2)$ unit cell was used. Configurations with the sulfur atom in the atop, long-bridge, and quasithreefold sites were separately optimized in order to find the lowest energy structure. Once the binding site was determined with the $c(2\times2)$ cell, the corresponding $\begin{bmatrix} 2 & \bar{2} \\ 1 & 1 \end{bmatrix}$ cell was then optimized starting with S at the $c(2\times2)$ binding site as the initial guess.

STM images were obtained from the electronic-structure calculations using modified Tersoff-Hamann theory.[14,15] The Tersoff-Hamann model for calculating the tunneling current assumes that the tip is a point source with an orbital of *s* character. In this case, the tunneling current is proportional to the density of states at the Fermi level. Extensions by Chen[16] to this theory allow the calculation of the tunneling current assuming *p* or *d* character orbitals at the tip, which we have also incorporated into our modeling.

EXPERIMENT

All experiments were performed in an ultrahigh-vacuum chamber with a base pressure $<2.0\times10^{-10}$ torr described in detail elsewhere.[17] The chamber is equipped for Auger electron spectroscopy (Physical Electronics), mass spectrometry (UTI), rear-view, low-energy electron diffraction (Varian Vacuum Products), scanning tunneling microscopy (RHK Technology), and a sputter gun (Physical Electronics).

The surface was cleaned by oxygen cleaning at a pressure of 5.0×10^{-9} torr for 5 min at a sample temperature of 1200 K to remove carbon followed by sputtering with argon ions (Ar, 99.9999%, Matheson gas) to remove oxygen (5.0×10^{-5} torr, 2 kV, 2.5-μA sample current). Once the bulk was depleted of impurities via extensive repetitive cleaning, only Ar^+ sputtering cycles were used to remove any surface contamination. The sample was then annealed at 1400 K for 3 min. This protocol was repeated until a sharp (1×1) LEED pattern was obtained and no oxygen or carbon was detected in Auger electron spectra. STM data obtained under these conditions also showed that the surface was essentially free from impurities. The average terrace size observed with STM was $\sim$180 Å corresponding to a miscut of 0.7°.[17]

The $\begin{bmatrix} 2 & \bar{2} \\ 1 & 1 \end{bmatrix}$-sulfur overlayer[17,18] was prepared by dosing hydrogen sulfide (H_2S, 99.5%, Matheson gas) directly at the sample using a 0.25-in. OD stainless-steel tube positioned 0.25 in. from the sample. The surface was exposed to H_2S for 90 s at a pressure of 3.0×10^{-9} torr and a sample temperature of 1400 K followed by annealing at 1400 K for 30 s. This produced a sharp $\begin{bmatrix} 2 & \bar{2} \\ 1 & 1 \end{bmatrix}$-LEED pattern which has been previously described as corresponding to a 0.5-ML coverage.[1,2]

All STM images shown here were taken at room temperature using bias voltages between -10 and -100 mV and a tunneling current of 1 nA, using a Pt-Ir tip. Each data set is composed of two images, scan left and scan right, which correspond to data collected from scanning the tip from left to right and right to left, respectively. The total time required for each constant current data set ranged from 51 s for $50\times50\,\text{nm}^2$ images to 4 min for $200\times200\,\text{nm}^2$ images. Within each experiment we sampled several regions over a $1\times1\,\mu\text{m}^2$ area of the surface. The STM was calibrated in the X,Y directions using a highly ordered, pyrolytic graphite sample (Union Carbide) and in the Z direction by measuring the step height of a monatomic molybdenum step.[19]

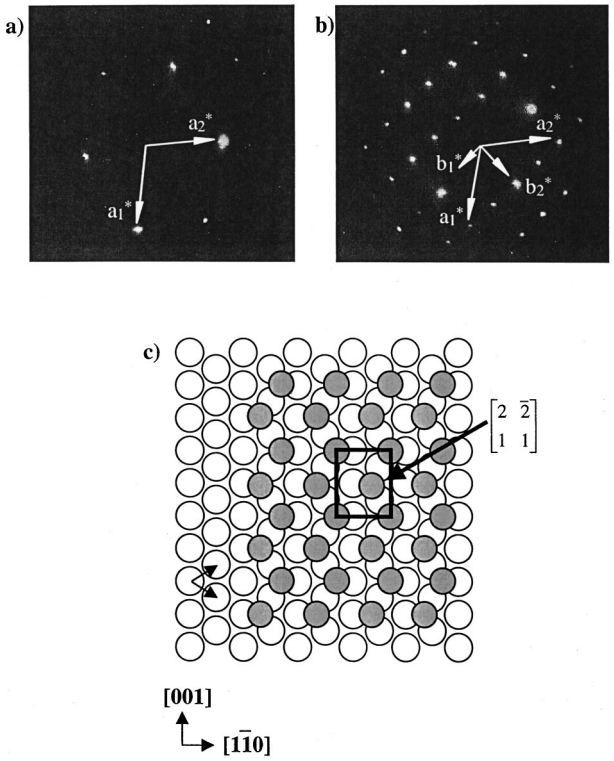

FIG. 1. Low-energy electron diffraction (LEED) patterns for (a) clean Mo(110) showing reciprocal-lattice vectors a_1^* and a_2^*, and (b) the 0.5-MI sulfur overlayer with reciprocal-lattice vectors for the overlayer structure, b_1^* and b_2^*; (c) a schematic of the overlayer real-space structure.

The crystallographic directions were determined from the LEED pattern, which yields the orientation of the crystal axes relative to the sample holder. The sample holder is fixed, therefore, by knowing the scan direction relative to the sample holder, and assuming step formation along a low index plane, the step orientation can be determined.

RESULTS

Experiment

Sulfur on Mo(110) forms a well-ordered $\begin{bmatrix} 2 & \bar{2} \\ 1 & 1 \end{bmatrix}$-LEED pattern at 0.5 ML (Fig. 1).[1,2] Analysis of this LEED pattern reveals a unit cell with dimensions of 6.30 Å along [001] and 4.45 Å along $[1\bar{1}0]$. However, atomically resolved STM imaging of this overlayer structure shows a structure with half the unit-cell size of that predicted by LEED. Specifically, the bright spots form rows along the [001] direction

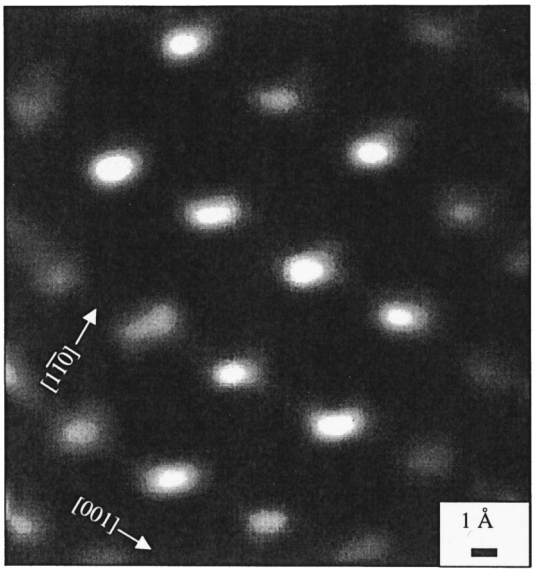

FIG. 2. Experimental STM image corresponding to the LEED pattern observed in Fig. 1.

with a separation of 3.1 ± 0.2 Å separated by 4.4 ± 0.2 Å along the $[1\bar{1}0]$ direction (Fig. 2).

The STM image of the overlayer appears to be a $c(2\times2)$ structure, in seeming contradiction to the LEED data. While the $c(2\times2)$ LEED spots are contained within the $\left[\begin{smallmatrix}2 & \bar{2}\\ 1 & 1\end{smallmatrix}\right]$ LEED spots, the presence of extra spots due uniquely to the $\left[\begin{smallmatrix}2 & \bar{2}\\ 1 & 1\end{smallmatrix}\right]$ structure indicates that there are large domains of the $\left[\begin{smallmatrix}2 & \bar{2}\\ 1 & 1\end{smallmatrix}\right]$ overlayer. Furthermore, no superposition of $c(2\times2)$ domains can give rise to the $\left[\begin{smallmatrix}2 & \bar{2}\\ 1 & 1\end{smallmatrix}\right]$ LEED structure. In addition, a large-area STM scan ($50\times50\,\mathrm{nm}^2$) shows that the STM image is the same over the entire surface (data not shown), demonstrating that there is no superposition of $\left[\begin{smallmatrix}2 & \bar{2}\\ 1 & 1\end{smallmatrix}\right]$ and $c(2\times2)$ domains. One possible explanation for the apparent inconsistency between the STM and LEED data is that the bright spots in the STM image do not correspond to the actual positions of the sulfur atoms. This point will be addressed in the following sections.

Density-functional studies of Mo(110)-$c(2\times2)$-S and Mo(110)-$\left[\begin{smallmatrix}2 & \bar{2}\\ 1 & 1\end{smallmatrix}\right]$-S

The most favorable binding site for a $c(2\times2)$ array of S adatoms at a 0.5-ML coverage on Mo(110) is displaced off of the long-bridge site by 0.35 Å toward the low-symmetry quasithreefold site, based on energy optimization of the atomic positions [Fig. 3(a)]. The binding energy for this site is -5.77 eV. Placing sulfur directly on the long-bridge site gives a slightly higher binding energy; however, it is indistinguishable from the off-long-bridge site within the error of the calculation (±0.1 eV). Sulfur bonding at the atop site is distinctly less favorable, with a binding energy of -3.92 eV.

Structural relaxation of the $\left[\begin{smallmatrix}2 & \bar{2}\\ 1 & 1\end{smallmatrix}\right]$ overlayer of sulfur on Mo(110) leads to a binding site 0.56 Å off of the long-bridge site in the threefold site and a binding energy of -6.08 eV [Fig. 3(b)]. Therefore, the $\left[\begin{smallmatrix}2 & \bar{2}\\ 1 & 1\end{smallmatrix}\right]$ configuration is favored over the $c(2\times2)$ by 0.31 eV. Note that the high-symmetry sites, the atop, and the long-bridge sites are not allowed in the $\left[\begin{smallmatrix}2 & \bar{2}\\ 1 & 1\end{smallmatrix}\right]$ overlayer because of symmetry constraints. If sulfur were placed in the atop or long-bridge sites, only the $c(2\times2)$ or (2×1) configurations are possible for a coverage of 0.5 ML. The optimal threefold binding site for S in the $\left[\begin{smallmatrix}2 & \bar{2}\\ 1 & 1\end{smallmatrix}\right]$ layer has nearly equal bond lengths to three surface Mo atoms, 2.38, 2.38, and 2.39 Å (Fig. 3). The sulfur-sulfur separation is 3.34 Å. The analogous bond distances in the $c(2\times2)$ overlayer are Mo-S bond lengths of 2.37, 2.37, and 2.46 Å, and a sulfur-sulfur separation of 3.15 Å. There is negligible relaxation perpendicular to the surface for the $\left[\begin{smallmatrix}2 & \bar{2}\\ 1 & 1\end{smallmatrix}\right]$ configuration, about 0.02 Å in the top layer and 0.08 Å in the second Mo layer. This is in contrast to a more pronounced buckling for the $c(2\times2)$ system, where there is a relaxation of 0.1 Å in the top layer and 0.08 Å in the second layer for this system. In addition, the adsorption of sulfur reduces the top-layer contraction of the Mo surface: -1.1% with sulfur adsorbed, compared to -7% for the clean surface.

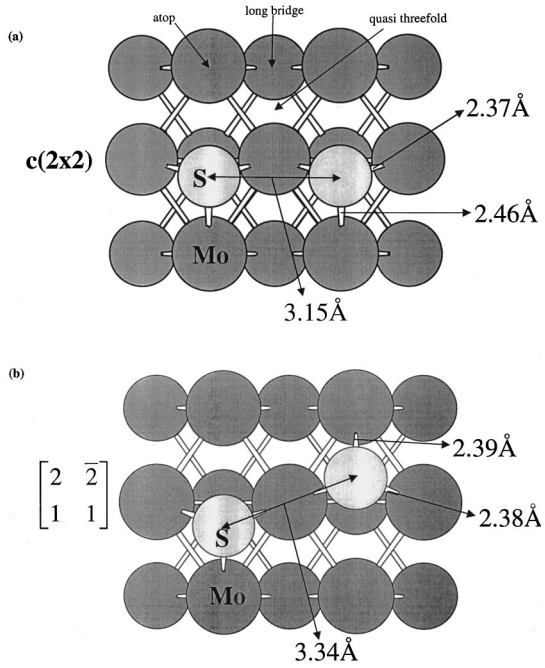

FIG. 3. Schematic of calculated, optimized sulfur positions on Mo(110) for (a) a $c(2\times2)$ array and (b) a $\left[\begin{smallmatrix}2 & \bar{2}\\ 1 & 1\end{smallmatrix}\right]$ structure.

These structural parameters can be compared with a tensor LEED study of the 0.25-ML $p(2\times2)$ sulfur overlayer on Mo(110) performed by Toofan *et al.*[4] The optimal binding site of the sulfur is shifted by 0.03 Å off the long-bridge site towards the quasithreefold site. This is qualitatively similar to the calculated results for the adsorption site for sulfur on the $c(2\times2)$ and $\left[\begin{smallmatrix}2 & \bar{2}\\ 1 & 1\end{smallmatrix}\right]$ overlayer structures.

Scanning tunneling microscopy simulations

Scanning tunneling microscopy images were generated from the calculated density of states and wave functions for Mo(110)-$\left[\begin{smallmatrix}2 & \bar{2}\\ 1 & 1\end{smallmatrix}\right]$-S, using a height of 3 Å, with s,p, or d orbitals as the tip (Fig. 4). These simulations show that the images depend on the tip states in agreement with other

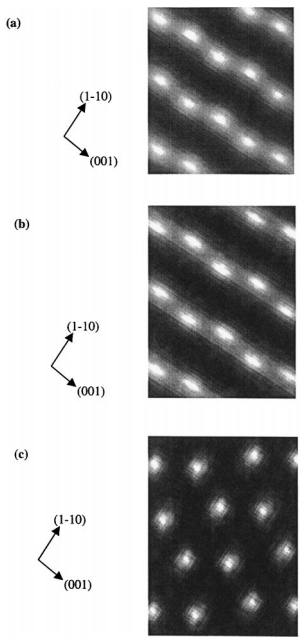

FIG. 4. Calculated STM images with (a) s, (b) p_z, and (c) d_{z^2} orbitals at the tip.

work. In the calculated STM images when using the s or p orbitals for the tip, the bright spots *do not* correspond to the positions of the sulfur atoms. In contrast, the simulated STM images for the Mo(110)-$c(2\times2)$-S have bright spots that correspond exactly to the atomic positions. Figure 5 shows the STM image of one unit cell of the $\left[\begin{smallmatrix}2 & \bar{2}\\ 1 & 1\end{smallmatrix}\right]$ configuration using s and p tip orbitals, in which the actual positions of the sulfur as well as the apparent center of the bright spot are marked. The bright spot is displaced from the position of the sulfur towards the long-bridge binding site; the net result is that the calculated STM image lessens the in-plane ''zigzag'' nature of the $\left[\begin{smallmatrix}2 & \bar{2}\\ 1 & 1\end{smallmatrix}\right]$ structure so that it begins to resemble the $c(2\times2)$ structure. In contrast, when using the d_{z^2} orbital on the tip, the bright spots correspond exactly to the atomic sulfur positions. It is important to note that the displacement of the bright spots occurs only under the specific conditions of zero bias; otherwise, the image produced does reveal bright spots on the sulfur positions. Notably, the experimental images were obtained at low bias voltage.

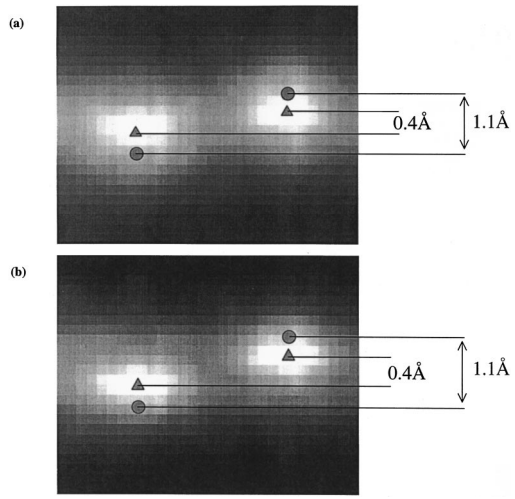

FIG. 5. One unit cell of the calculated STM image of $\left[\begin{smallmatrix}2 & \bar{2}\\ 1 & 1\end{smallmatrix}\right]$-S/Mo(110) showing the actual atomic position of sulfur (circle) and the center of the bright spot (triangle) with (a) s and (b) p_z orbitals at the tip. The image with the d_{z^2} orbital at the tip has spots directly above the sulfur atomic positions.

Discussion

Our calculations confirm that the stability of the $\left[\begin{smallmatrix}2 & \bar{2}\\ 1 & 1\end{smallmatrix}\right]$-S overlayer is energetically favored over the $c(2\times2)$-S overlayer on Mo(110) due to a delicate balance of several factors. We interpret our results in terms of a balance between the chemical bonding between the surface Mo atoms and the sulfur adatoms, and electrostatic repulsion caused by the interaction of nearby dipoles.

Electrostatic repulsion arises from chemical bonding that leads to transfer of electron density from Mo to the sulfur atom. Experimentally, the degree of charge transfer can be estimated based on changes in the work function of the surface induced by sulfur adsorption on the Mo surface. For example, a dipole of 0.08 D is created at the surface when 0.5 ML of S is adsorbed on Mo(110), based on experimental work-function change measurements.[20] The dipoles created by sulfur bonding repel each other, leading to an overall increase in the total energy. At higher coverages of sulfur, there will be more electrostatic repulsion, because the sulfurs are closer together. This is offset by the energy gained by forming Mo-S bonds.

It would be interesting to determine whether or not it is the electrostatic repulsion which determines the surface structure of 0.5 ML of sulfur on Mo(110). The optimization of the $c(2\times2)$ structure reveals the position of greatest *chemical* bonding, as the electrostatic repulsion is held constant by the unit-cell geometry. On the other hand, in the $\left[\begin{smallmatrix}2 & \bar{2}\\ 1 & 1\end{smallmatrix}\right]$ structure there is freedom in the sulfur-sulfur atomic distance, and the sulfur atoms rearrange so that the total energy is minimized; the sulfur atoms are 0.2 Å further apart than in the $c(2\times2)$ case. This reduces the electrostatic repulsion, since the interaction between dipoles drops off as $1/d^3$, with distance d. There is also a decrease in the degree of buckling in the $\left[\begin{smallmatrix}2 & \bar{2}\\ 1 & 1\end{smallmatrix}\right]$ system, however, as compared to the $c(2\times2)$. The difference in buckling necessarily corresponds to differences in metal-metal bonding which, in turn, will contribute to the total energies of the two configurations.

Changes in dipole-dipole repulsion cannot account for the difference in stability of the $\left[\begin{smallmatrix}2 & \bar{2}\\ 1 & 1\end{smallmatrix}\right]$-S phase compared to the hypothetical $c(2\times2)$-S structure. If we assume that all of the calculated energy difference between the $\left[\begin{smallmatrix}2 & \bar{2}\\ 1 & 1\end{smallmatrix}\right]$ and $c(2\times2)$ systems is due to electrostatic repulsion and that there are six dipole-dipole interactions per unit cell of the $\left[\begin{smallmatrix}2 & \bar{2}\\ 1 & 1\end{smallmatrix}\right]$ overlayer, a dipole moment of 4.3 D would be necessary to account for the energy difference in the two configurations, a value two orders of magnitude larger than the value of 0.08 D derived from work-function change measurements. Therefore, we conclude that changes in chemical bonding largely determine the stability of the $\left[\begin{smallmatrix}2 & \bar{2}\\ 1 & 1\end{smallmatrix}\right]$ sulfur overlayer in relation to the $c(2\times2)$ configuration.

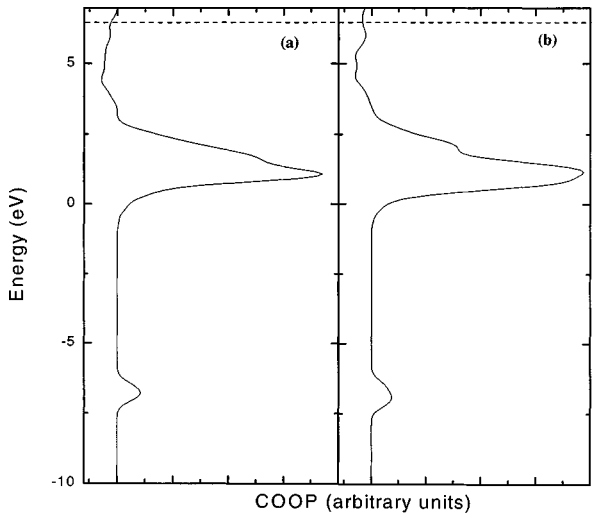

FIG. 6. Crystal orbital overlap population (COOP) plots of the Mo $4d-$S $2p$ orbital interaction for (a) $c(2\times2)$ sulfur overlayer and (b) $[\bar{2}\ 2;1\ 1]$ sulfur overlayer. Both plots are on the same scale for comparison.

Differences in local Mo-S bonding are also not responsible for differences in stability between the two overlayers either. As is well established for bonding of S and O to metal surfaces, the bonding between the sulfur adatom and the Mo atoms takes place through the S $3p$ and the Mo $4d$ orbitals. By comparing the S-Mo interaction, we can determine the differences in the strength of the S-Mo bond between the two cases. An analysis of the S-Mo bonding using the crystal orbital overlap population (COOP) (Ref. 21) between the S $3p$ and Mo $4d$ orbitals shows that the bonding is virtually identical in the $c(2\times2)$ and $[\bar{2}\ 2;1\ 1]$ cases (Fig. 6); the strength of the S-Mo bond plays no role in the energy difference between the two different overlayers.

We attribute the difference in stability of the $c(2\times2)$ and $[\bar{2}\ 2;1\ 1]$ configurations of sulfur to differences in metal-metal bonding. In the $c(2\times2)$ case, there is a pronounced buckling of the surface Mo atoms of 0.1 Å, in contrast to the small 0.02 Å buckling for the $[\bar{2}\ 2;1\ 1]$ case. The long-bridge Mo atoms are pushed into the surface by the presence of the sulfur atom; this is similar to the buckling observed for a sulfur overlayer on Mo(100), where the second-layer Mo atoms are also pushed into the substrate by the sulfur atoms. The buckling occurs for the $c(2\times2)$ configuration because all the sulfur atoms are closer to the long-bridge Mo atoms, whereas in the $[\bar{2}\ 2;1\ 1]$ configuration the sulfur is bound with equal bond lengths to three Mo atoms, which reduces the buckling in this case. This result demonstrates that changes in metal-metal bonding can override other considerations in determining the stability of certain surface structures. Similar conclusions have been found for sulfur adsorbed on Re(0001), where combined LEED and STM studies showed that the buckling of the surface atoms depended on the sulfur coverage.[22] In contrast to our results, however, it was found for the sulfur on Re(0001) system that the buckling was greater for higher coverages of sulfur.

In addition to providing insight into the reason for the enhanced stability of the $[\bar{2}\ 2;1\ 1]$ versus the $c(2\times2)$ configuration, our calculations also provide some understanding of the discrepancy between the LEED and STM results and underscore the importance of theoretical modeling of STM images. The experimental STM image of the LEED-identified Mo(110)-$[\bar{2}\ 2;1\ 1]$-S structure resembles what one would expect for the $c(2\times2)$ configuration, with straight rows of bright spots instead of the zigzag pattern characteristic of the $[\bar{2}\ 2;1\ 1]$ structure. However, our simulations indicate that the bright spots do not correspond to the atomic sulfur positions, but instead are displaced towards the long-bridge site for tunneling to s and p_z tip states. The net result is that the amplitude of the zigzag is reduced; while this amplitude is 1.1 Å if one considers the atomic positions, this oscillation is reduced to just 0.4 Å in the calculated STM images. The lateral resolution observed in STM depends on both the radius of curvature of the STM tip and the noise in the x,y signals applied to the piezoelectric scanner. Typically, for metal systems the lateral resolution is greater than 1 Å.[15,23] Therefore, this difference in position is too small to be resolved experimentally, explaining the observed STM image.

The reduction in the reduced amplitude of the zigzag pattern in the calculated and observed STM images of the $[\bar{2}\ 2;1\ 1]$ structure can be traced to an occupied surface orbital 0.04 eV below the Fermi level. This is a bonding orbital between the third (not bridging) Mo atom and a p orbital of the sulfur atom, and has lobes of electron density that are localized away from and above the sulfur atom in the direction of the long-bridge site. It is these lobes that are imaged in the calculated STM images, which explains the apparent reduced amplitude of displacement in the $[\bar{2}\ 2;1\ 1]$ structure. Because we find that this image is dominated by an orbital that is near the Fermi level, we predict that the in-plane corrugation of the $[\bar{2}\ 2;1\ 1]$ structure should be observed if the bias voltage is increased so that this particular orbital does not contribute significantly to the tunneling current.

Since the experimental images resemble most the calculated images obtained with the s or p_z orbitals at the tip, we conclude that it is these orbitals which primarily contribute to the tunneling current. Although the d orbitals have the largest density of states near the Fermi level, out of the d orbitals only d_{z^2} orbitals should contribute to the tunneling current. Moreover, there are also s and p states in close energy proximity with the d states of Pt, so there will be a contribution from these states as well. In addition, because the s and p_z orbitals have a greater spatial extent than the d_{z^2} orbital, a greater interaction of these orbitals with the surface wave functions is expected.

The combination of experimental and simulated STM images has been previously used on several related systems, including Rh(111)+$c(4\times2)$-2S,[24] Re(0001)-$p(2\times2)$-S,[25] and Mo(100)-$c(4\times2)$-S,[26] to elucidate structural details. These studies used semiempirical extended Hückel theory to treat the system and the tip together, allowing for a complete treatment of the tip-sample interaction. For example, experimental STM images of the Rh(111)+$c(4\times2)$-2S system were elucidated using simulations that found that sulfur in hcp sites and sulfur in fcc sites gave rise to different kinds of maxima in the STM image. One disadvantage in using extended Hückel theory to model these systems is the inability

to perform structural optimizations. This limits simulations to systems whose structural parameters have been determined independently. *Ab initio* methods allow the determination of detailed structures and thus STM simulations of a wider variety of systems are possible. Moreover, surface relaxations potentially affect the resulting STM image. As has been shown for sulfur on Re(0001), there are differences in the STM images which are caused by the positions of the substrate atoms.[27] Therefore, the ability to accurately predict surface relaxations with theoretical methods is important in comparing with experimental results.

One factor that is not taken into account in our STM simulated images is the interaction of the tip with the surface. While tip-surface interactions are in general weak for typical tip-sample separations, the shape as well as the composition of the tip can have an effect on the STM image. Sautet *et al.* have investigated these effects using a combination of scattering theory and a semiempirical extended Hückel theory.[25] They found for a sulfur overlayer on Re(0001) that the different experimentally observed STM images could be explained by modeling the tip termination as a single atom or a small cluster of atoms. In our case we do not consider the geometry of the tip, and assume that it is a point source. Tip geometry effects can clearly be important for some systems, and will be considered in future work.

ACKNOWLEDGMENT

The authors would like to thank Ryoka Systems, Inc. for its support of this work.

*Electronic address: friend@chemistry.harvard.edu

[1] W. Witt and E. Bauer, Ber. Bunsenges. Phys. Chem. **90**, 248 (1986).
[2] A. Sanchez *et al.*, Surf. Sci. **171**, 157 (1986).
[3] L. Peralta, Y. Berthier, and J. Oudar, Surf. Sci. **55**, 199 (1976).
[4] J. Toofan, G. R. Tinseth, and P. R. Watson, J. Vac. Sci. Technol. A **12**, 2246 (1994).
[5] CASTEP, version 3.8, Molecular Simulations, Inc., 1998.
[6] M. C. Payne *et al.*, Rev. Mod. Phys. **64**, 1046 (1992).
[7] D. Vanderbilt, Phys. Rev. B **41**, 7892 (1990).
[8] K. Laasonen *et al.*, Phys. Rev. B **47**, 10 142 (1993).
[9] J. P. Perdew and A. Zunger, Phys. Rev. B **23**, 5048 (1981).
[10] G. Kresse and J. Furthmuller, Phys. Rev. B **54**, 11 169 (1996).
[11] G. Kresse and J. Furthmuller, Comput. Mater. Sci. **6**, 15 (1996).
[12] B. Kohler *et al.*, Phys. Rev. Lett. **74**, 1387 (1995).
[13] M. Methfessel, D. Hennig, and M. Scheffler, Phys. Rev. B **46**, 4816 (1992).
[14] J. Tersoff and D. R. Hamann, Phys. Rev. Lett. **50**, 1998 (1983).
[15] J. Tersoff and D. R. Hamann, Phys. Rev. B **31**, 805 (1985).
[16] C. J. Chen, Phys. Rev. B **42**, 8841 (1990).
[17] P. G. Clark, Jr. and C. M. Friend (unpublished).
[18] The $\left[\begin{smallmatrix} 2 & \bar{2} \\ 1 & 1 \end{smallmatrix}\right]$-sulfur overlayer has been previously referred to as the ''4×1'' overlayer.
[19] L. M. de la Garza and L. J. Clarke, J. Phys. C **14**, 5391 (1981).
[20] P. G. Clark, Jr. and C. M. Friend, Surf. Sci. (unpublished).
[21] R. Hoffmann, *Solids and Surfaces: A Chemist's View of Bonding in Extended Structures* (VCH, New York, 1988).
[22] A. Barbieri *et al.*, Surf. Sci. **312**, 10 (1994).
[23] C. J. Chen, *Introduction to Scanning Tunneling Microscopy* (Oxford University Press, New York, 1993).
[24] J. Cerdá *et al.*, Phys. Rev. B **56**, 15 900 (1997).
[25] P. Sautet *et al.*, Surf. Sci. **295**, 347 (1993).
[26] J. C. Dunphy, P. Sautet, and M. Salmeron, Surf. Sci. **364**, 335 (1996).
[27] J. Cerdá *et al.*, Surf. Sci. **409**, 145 (1998).